

Development of a technique for modelling clay liner desiccation

Y. Zhou¹ and R. Kerry Rowe^{2,*†}

¹*Climate Control Systems, Visteon Corporation, 45000 Helm Street, Plymouth, MI 48170, USA*

²*GeoEngineering Centre at Queen's-RMC, Department of Civil Engineering, Queen's University, Ellis Hall, Kingston, ON, K7L 3N6 Canada*

SUMMARY

This paper presents a model for the analysis of clay liner desiccation in a landfill barrier system due to temperature effects. The model incorporates consideration of fully coupled heat-moisture-air flow, a non-linear constitutive relationship, the dependence of void ratio and volumetric water content on stress, capillary pressure and temperature, and the effect of mechanical deformation on all governing equations. Mass conservative numerical schemes are proposed to improve the accuracy of the finite element solution to the governing equations. The application of the model is then demonstrated by examining three test problems, including isothermal infiltration, heat conduction and non-isothermal water and heat transport. Comparisons are made with results from literature, and good agreement is observed. Copyright © 2003 John Wiley & Sons, Ltd.

KEY WORDS: clay liner; desiccation; numerical modelling; temperature; unsaturated flow

1. INTRODUCTION

Clay liners form an integral part of the barrier system for most modern waste disposal facilities [1]. The low hydraulic conductivity of the liner serves to minimize advective flow of leachate from the landfill. When combined with a geomembrane to form a composite liner, the clay liner also serves to minimize leachate through any holes or defects in the geomembrane. Furthermore, in the case of a composite liner, the clay liner component provides a backup to control the escape of fluids when the service life of the geomembrane is reached. Well constructed clay liners are considered to have an indefinite service life [2,3] provided that they remain intact and uncracked for the contaminating life span of the landfill (i.e. the period of time during which leachate escape could have an adverse effect on groundwater). This then raises the question as to what effect the temperature generated in the landfill, and presence of an

*Correspondence to: R. K. Rowe, GeoEngineering Centre at Queen's-RMC, Department of Civil Engineering, Queen's University, Ellis Hall, Kingston, ON, K7L 3N6 Canada.

†E-mail: kerry@civil.queensu.ca

Contract/grant sponsor: Natural Sciences and Engineering Research Council of Canada (NSERC), Terrafix Geosynthetic Inc.

Contract/grant sponsor: Centre for Research in Earth and Space Technology (CRESTech)

*Received 27 March 2002
Revised 23 December 2002*

essentially impermeable geomembrane liner, above the clay liner may have on the long-term performance of the clay liner.

Significant temperature increases may occur above landfill liners due to the biodegradation of organic matter in the waste body. Measured temperatures on the liner system ranging from 10 to 65°C have been reported [2–7].

The properties of soil material vary with temperature. For example, as temperature increases, both the hydraulic conductivity and diffusion coefficient increase. According to Collins [4], both the hydraulic conductivity and diffusion coefficient at 60°C are three times higher as those at 10°C.

Under non-isothermal conditions, the temperature gradient and capillary pressure gradient are two driving forces for moisture transport in clay liner systems. When a temperature gradient is applied on an unsaturated landfill liner system (Figure 1), it causes changes in water and air pressures in the medium. Liquid water moves from higher capillary pressure towards lower capillary pressure, vapour water moves from higher temperature towards lower temperature area due to vapour diffusion. In the unsaturated system, air moves from higher air pressure to lower air pressure area. Air flow can increase or decrease vapour transport due to advection. The combined effect of liquid water, vapour water and air flow is a redistribution of water in the liner system; this redistribution has the potential to cause desiccation of the clay liner in the area of higher temperature.

The consequences of desiccation are reductions in void ratio, deformation and volume change, crack initiation and propagation [8]. A significant temperature increase could cause significant loss of water content and induce cracks in clay liners in a short period of time (a few years), that could substantially increase the hydraulic conductivity of the liner or cracked zone. Several theoretical models have been proposed for analysing the desiccation and cracking of soil under *isothermal* conditions. For example, Lee *et al.* [9] proposed a finite element model of crack propagation in brittle soils based on the linear elastic fracture mechanics theory and the propagation fracture toughness parameter criterion. Morris *et al.* [10] developed a theoretical model for one-dimensional analysis of crack depth in unsaturated soils using three different approaches: (1) elasticity, (2) linear elastic fracture mechanics and (3) strength theory. Konrad

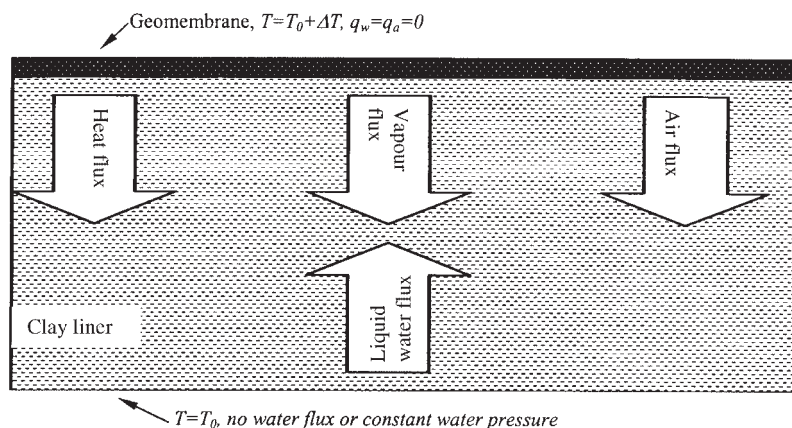


Figure 1. Heat and mass fluxes in an unsaturated medium under a geomembrane due to a temperature gradient.

and Ayad [11] proposed a general theory for the analysis of cohesive soils undergoing desiccation, with special attention to cracks resulting from a moisture content reduction induced by evaporation from the surface of clayey soils. The model can predict the depth and spacing of primary cracks using the theory of linear elastic fracture mechanics and the fictitious stress superposition concept.

Under *non-isothermal* condition, models developed by Philip and de Vries [12] and Milly [13] have been widely used in engineering practice for moisture transport under temperature effects in *rigid* porous media. Philip and de Vries model uses temperature and water content as basic variables, while Milly's model uses temperature and capillary pressure as basic variables. The limitations of Philip and de Vries model include the assumptions of homogeneous medium, no hysteretic effect, and unsaturated media. The water content based Philip and de Vries model is not applicable to saturated media, since water content is unchanged in saturated cases. By expressing the governing equations in terms of temperature and capillary pressure, Milly's model has eliminated the above-mentioned restrictions of the Philip and de Vries model. However, the deformation of porous media was not considered in either of these models.

Döll [14,15] studied desiccation of mineral liners below landfills with heat generation using Milly's model. She evaluated the effects of hydraulic conductivity, position of the water table and temperature on the predicted profiles of water content and capillary pressure. The probability of liner cracking was discussed based on the calculated suction profiles. Döll's finite difference software was developed for one-dimensional conditions. Heibroek [16] proposed a method for calculating the non-isothermal stress field in clay liners by first using Döll's model to calculate suction profile in the liner, then using the model proposed by Morris *et al.* [10] to calculate tensile horizontal stress and evaluate the possibility of tensile failure.

While Döll's study represented a useful advance, it was limited by virtue of the fact that no consideration was given to: (a) the effect of stress and deformation, (b) air flow, (c) temperature on hydraulic conductivity and the water retention curve other than due to changes in surface tension and viscosity, and (d) hysteretic effects. Furthermore, there is some question as to how to determine the vapour transport enhancement factor F_v used in Döll's model. In Döll's case studies, a wide range of different F_v values were needed in order to obtain a reasonable fit to experimental data. The model by Morris *et al.* [10] for crack analysis is valid for isothermal media. Heibroek's [16] extension to the non-isothermal case is a semi-coupled approach that neglects the effect of temperature on deformation and therefore the tensile stress field. Since the thermal stress due to thermal expansion of the medium is an important part of the stress field, and may not be negligible, there is a need to examine this effect.

In recent years, a great deal of work has been done to study heat and mass transfer in *deformable* unsaturated porous media [17–22]. Geraminegad and Saxena [18] developed a thermoelastic model for saturated and unsaturated porous media incorporating soil deformation due to changes in the flowing phases (i.e. moisture and air phases), but did not include soil deformation due to external loading. Thomas and He [20], and Thomas *et al.* [23] presented models for coupled deformations and heat and moisture flow in unsaturated media using the theory of elasticity/elasto-plasticity and a state surface approach. Yang *et al.* [21] proposed a general three-dimensional mathematical model for coupled heat, moisture, air flow and deformation problems in unsaturated soils. An elastoplastic framework was used to describe the deformation behaviour of the unsaturated soil structure. Zhou *et al.* [22] proposed a consistent fully coupled nonlinear model for heat, moisture and air transfer in deformable unsaturated media based on two general constitutive relationships relating void ratio and liquid water

content to stress, capillary pressure and temperature change. The governing equations are explicitly expressed in terms of deformation, capillary pressure, air pressure and temperature. The model takes into consideration thermo-osmosis and thermal-filtration (thermodynamically coupled effects), stress and temperature effects on water retention curve, moisture retention hysteresis and soil inhomogeneities, the heat of wetting, heat sink due to thermal expansion of the unsaturated medium, phase change between liquid water and vapour water, and compressibility of liquid water.

An important characteristic of clay liner materials used in landfills is their deformation due to thermal, hydraulic and external loading (such as overburden pressure). Strong coupling is expected between deformation and moisture transfer [23]. A model that includes this coupling makes it possible to quantitatively investigate its significance.

Mass balance error is a problem often encountered in numerical modelling of mass transport phenomenon using capillary potential (or suction) as a basic variable. In transient analyses the error can accumulate to unacceptable levels [24]. Abriola and Rathfelder [25] studied the causes of mass balance errors in modelling two phase immiscible flows in rigid media. They concluded that the mass balance errors in traditional finite element pressure-based models result from failure to properly evaluate the capacity coefficients when the capillary pressure-saturation relationship is nonlinear, and suggested that conservation of mass can be obtained when the capacity coefficient is formulated to preserve the elemental approximation of the derivative of water saturation with respect to time. Döll [14,15] studied moisture and heat transfer using mass-conservative one-dimensional finite difference scheme. To the authors' knowledge, until now, no mass-conservative numerical scheme has been proposed for use in the finite element analysis of moisture and heat transfer in deformable unsaturated soils.

The objective of this paper is to develop a theoretical model to study heat and moisture transfer in landfill liner systems and evaluate the potential of desiccation cracking by examining the resulting stress field. One of the major differences between this and previous studies is that in this study a fully coupled model is used to assess the effects of temperature and thermal consolidation on moisture transfer. Using this model, stress and deformation can be simultaneously calculated to facilitate the study of desiccation cracking. Temperature effects on stresses, and the effect of air flow on moisture redistribution are also considered. New mass-conservative finite element schemes are proposed to obtain mass balance results and accurate solutions. A set of numerical examples are presented and compared with other analytical and numerical solutions to demonstrate the validity of the finite element technique.

The following section summarizes the complete set of fully coupled governing equations needed to consider the aforementioned coupling effects.

2. THEORETICAL MODEL

In a non-isothermal unsaturated soil medium, there are three different phases (solid, liquid and gases) and three different physical processes (deformation, mass flow and heat transfer) to be considered. To establish the governing equations needed to describe the interactions between phase and processes, the following assumptions are made: (1) soil medium is isotropic, (2) small deformation and infinitesimal strain, (3) thermal equilibrium between different phases, (4) liquid water and air flow both follow Darcy's law, (5) vapour flow is due to both diffusion and convection and (6) heat flow is due to conduction, convection, and latent heat transfer. Creep is

neglected and the initial strain is considered to be zero. Due to limited data, the effects of thermo-osmosis and thermal-filtration are not considered in this study.

The following two constitutive relationships (in general form) relating void ratio (e) and liquid water content (θ) to net mean stress (σ^*), capillary pressure (p_c) and temperature increase (T) are introduced into the simultaneous governing equations:

$$e = f(\sigma^*, p_c, T) \quad (1)$$

$$\theta = f(\sigma^*, p_c, T) \quad (2)$$

where $p_c = p_l - p_a$, $\sigma^* = (\sigma_1 + \sigma_2 + \sigma_3)/3 + p_a$, p_l is pore water pressure, p_a is air pressure and σ_i ($i = 1, \dots, 3$) are the three principal stresses (tension positive).

From Equation (1), the volumetric strain (ε_v) of soil material can be derived as

$$d\varepsilon_v = \frac{de}{1 + e_0} = \frac{d\sigma^*}{K} + B_1 dp_c + B_2 dT \quad (3)$$

where

$$K = \frac{1}{1 + e_0} \frac{\partial e}{\partial \sigma^*}, \quad B_1 = \frac{1}{1 + e_0} \frac{\partial e}{\partial p_c}, \quad B_2 = \frac{1}{1 + e_0} \frac{\partial e}{\partial T} \quad (4)$$

e_0 is initial void ratio and K is bulk modulus of the soil medium, B_1 is compressibility of the soil medium due to capillary pressure change, B_2 is thermal expansion coefficient.

In the case of non-linear thermoporoelastic medium, the following complete stress-strain relationship can be established from Equation (3) in incremental form as

$$d\sigma_{ij} = 2G \left(d\varepsilon_{ij} + \delta_{ij} \frac{\mu}{1 - 2\mu} d\varepsilon_{kk} \right) - KB_1 \delta_{ij} dp_c - \delta_{ij} dp_a - KB_2 \delta_{ij} dT \quad (5)$$

where σ_{ij} is stress tensor, ε_{ij} is strain tensor, δ_{ij} is Kronecker's delta, G is shear modulus and μ is Poisson's ratio.

Assuming elastic isotropy, K , G and μ are related by

$$\mu = \frac{3K - 2G}{6K + 2G} \quad (6)$$

The equation for force equilibrium in the soil can be written in incremental form as

$$(d\sigma_{ij})_j + db_i = 0 \quad (7)$$

where b_i is body force in i direction.

In unsaturated soils, water exists in the pores in the forms of liquid water and water vapour. Liquid water is transported due to the capillary potential gradient, and can be described by Darcy's law. Water vapour is transported by diffusion and convection.

$$q_l = -\rho_l \kappa_l \nabla(p_c + p_a + \rho_l g z); \quad q_v = -D^* \nabla \rho_v + \rho_v v_a \quad (8)$$

where q_l and q_v are fluxes of liquid water and vapour water, respectively; κ_l is mobility coefficient of liquid water associated with Darcy's flow [$\kappa_l = K_l / (\rho_l g)$]; K_l is hydraulic conductivity of the soil medium, g is gravitational acceleration, ρ_l and ρ_v are densities of liquid water and water vapour, respectively, z is vertical co-ordinate, D^* is effective molecular diffusion coefficient of water vapour and v_a is velocity of air.

Both ρ_l and ρ_v depend on temperature and capillary pressure:

$$\rho_l = \rho_{l0}[1 + \beta_1(p_c + p_a) - \alpha_1 T] \quad (9)$$

$$\rho_v = \rho_0 h = \rho_0(T_K) \exp\left(\frac{p_c}{\rho_l R_v T_K}\right) \quad (10)$$

where ρ_{l0} is initial density of liquid water, β_1 is compressibility of liquid water, α_1 is thermal expansion coefficient of liquid water, ρ_0 is density of vapour at saturation depending on temperature, h is relative humidity, $T_K (= T_{0K} + T)$ is current temperature in °K; $T_{0K} (= T_0 + 273.15)$ is reference temperature in °K; T_0 is reference temperature in °C and R_v is the gas constant for vapour.

Velocity of air can be described by Darcy's law (neglecting the gravitational contribution):

$$v_a = -\kappa_a \nabla p_a \quad (11)$$

where κ_a is the mobility coefficient of air. Both κ_l and κ_a depend on the intrinsic permeability of the soil material, degree of saturation and temperature.

The mass balance for water in a deformable unsaturated soil is given by

$$\frac{\partial\{\rho_l(1+e)\theta + \rho_v[e - (1+e)\theta]\}}{(1+e_0)\partial t} = -\nabla(q_l + q_v) \quad (12)$$

The mass balance for air in a deformable unsaturated soil can be expressed as

$$\frac{\partial\{\rho_{da}[e - (1-H)(1+e)\theta]\}}{(1+e_0)\partial t} = -\nabla q_{da} \quad (13)$$

where t is time, ρ_{da} is the density of dry air, H is the coefficient of solubility of air in water defined by Henry's law [26] and q_{da} is dry air flux due to solubility and convection and is given by

$$q_{da} = \frac{H\rho_{da}}{\rho_l} q_l + \rho_{da} v_a \quad (14)$$

Dry air density ρ_{da} in an unsaturated soil is related to air pressure, temperature and vapour density:

$$\rho_{da} = \frac{p_a}{R_{da} T_K} - \frac{R_v}{R_{da}} \rho_v \quad (15)$$

where R_{da} is the gas constant of dry air.

In a non-isothermal unsaturated soil medium, assuming thermal equilibrium is maintained between different phases, the total heat flux (q_T) is due to heat conduction, heat convection and latent heat transfer, and can be expressed as

$$q_T = -\lambda' \nabla T + q_l C_l T + q_v C_v T + q_{da} C_{da} T + L_0 q_v \quad (16)$$

where λ' is Fourier thermal conductivity of the unsaturated medium, C_l , C_v and C_{da} are the gravimetric specific heats of liquid water, water vapour and dry air respectively, L_0 is latent heat of evaporation at the reference temperature T_0 .

The heat energy balance can be described by

$$\frac{\partial \Phi}{(1+e_0)\partial t} - (T + T_0)KB_2 \frac{\partial \varepsilon_v}{\partial t} = -\nabla q_T \quad (17)$$

where Φ is the heat content of a representative element (specific volume = $1 + e$) of the medium, and can be expressed as

$$\begin{aligned} \Phi = & \{ \rho_s C_s + \rho_1 C_1 (1 + e) \theta + \rho_v C_v [e - (1 + e) \theta] + \rho_{da} C_{da} [e - (1 - H)(1 + e) \theta] \} T \\ & + L_0 \rho_v [e - (1 + e) \theta] + \rho_1 (1 + e) \theta W \end{aligned} \quad (18)$$

The second term in Equation (17) is the heat sink due to thermal expansion of the medium. W is the differential heat of wetting associated with the exothermic process of wetting of the porous medium.

The final mass balance equation for water (include liquid water and vapour water) can be written as

$$\begin{aligned} & (L_{11} + L_{21}) \frac{\partial \varepsilon_v}{\partial t} + (L_{12} + L_{22}) \frac{\partial p_c}{\partial t} + (L_{13} + L_{23}) \frac{\partial p_a}{\partial t} + (L_{14} + L_{24}) \frac{\partial T}{\partial t} \\ & = \nabla [(\rho_1 \kappa_1 + D_1^*) \nabla p_c] + \nabla [(\rho_1 \kappa_1 + \rho_v \kappa_a + D_2^*) \nabla p_a] + \nabla (D_3^* \nabla T) \\ & + \nabla [\rho_1 \kappa_1 \nabla (\rho_1 g z)] \end{aligned} \quad (19)$$

The mass balance equation for dry air is

$$\begin{aligned} L_{31} \frac{\partial \varepsilon_v}{\partial t} + L_{32} \frac{\partial p_c}{\partial t} + L_{33} \frac{\partial p_a}{\partial t} + L_{34} \frac{\partial T}{\partial t} = & \nabla (H \rho_{da} \kappa_1 \nabla p_c) + \nabla [\rho_{da} (\kappa_a + H \kappa_1) \nabla p_a] \\ & + \nabla [H \rho_{da} \kappa_1 \nabla (\rho_1 g z)] \end{aligned} \quad (20)$$

Finally the heat energy balance equation is

$$\begin{aligned} & L_{41} \frac{\partial \varepsilon_v}{\partial t} + L_{42} \frac{\partial p_c}{\partial t} + L_{43} \frac{\partial p_a}{\partial t} + L_{44} \frac{\partial T}{\partial t} \\ & = \nabla [D_{c2}^* \nabla p_c + D_{a2}^* \nabla p_a + D_{T2}^* \nabla T + (C_1 \rho_1 + C_{da} \rho_{da} H) \kappa_1 T \nabla (\rho_1 g z)] \end{aligned} \quad (21)$$

where L_{ij} , D_1^* , D_2^* , D_3^* , D_{c2}^* , T_{a2}^* and D_{T2}^* are given in Appendix A.

Equations (7), (19)–(21) are a set of fully coupled governing equations for the thermohydrromechanical behaviour of unsaturated soils expressed in terms of deformation, capillary pressure, air pressure and temperature. The non-linear nature of the governing partial differential equations makes it very difficult to obtain an analytical solution to these equations even for simple boundary conditions. However, numerical techniques (e.g. finite element and finite difference methods) can be used to obtain approximate solutions to problems with general initial and boundary conditions. In the following, the finite element method is used to solve the governing equation for the problem of interest.

3. MASS CONSERVATIVE FINITE ELEMENT SCHEME

Moisture and heat transfer in a landfill liner can usually be idealized as a one-dimensional problem. Consequently, a mass conservative finite element technique is developed in this section to obtain solution to the governing simultaneous equations. Vertical displacement (u), capillary pressure (p_c), air pressure (p_a) and temperature increase (T) are chosen as basic variables.

Application of the virtual work principle to the force equilibrium equation (7) and Petrov–Galerkin method to mass balance equations (19), (20) and the heat energy balance equation (21)

yield the following general matrix form of the finite element equations:

$$\begin{bmatrix} G_{11} & G_{12} & G_{13} & G_{14} \\ G_{21} & G_{22} & G_{23} & G_{24} \\ G_{31} & G_{32} & G_{33} & G_{34} \\ G_{41} & G_{42} & G_{43} & G_{44} \end{bmatrix} \begin{Bmatrix} \dot{u} \\ \dot{p}_c \\ \dot{p}_a \\ \dot{T} \end{Bmatrix} + \begin{bmatrix} 0 & 0 & 0 & 0 \\ 0 & K_{22} & K_{23} & K_{24} \\ 0 & K_{32} & K_{33} & 0 \\ 0 & K_{42} & K_{43} & K_{44} \end{bmatrix} \begin{Bmatrix} u \\ p_c \\ p_a \\ T \end{Bmatrix} = \begin{Bmatrix} \dot{F}_1 \\ F_2 \\ F_3 \\ F_4 \end{Bmatrix} \quad (22)$$

The coefficient matrices **G** and **K** depend on nodal variables. G_{ij} , K_{ij} and F_i ($i = 1, \dots, 4$; $j = 1, \dots, 4$) are given in Appendix B.

In order to obtain time domain solutions, the following single step time integration is introduced:

$$\int_{t_1}^{t_2} x(t) dt = (x_1 + \xi \Delta x) \Delta t \quad (23)$$

$$\int_{t_1}^{t_2} \dot{x}(t) dt = \Delta x \quad (24)$$

where t_1 and t_2 are two time instances, $\Delta t = t_2 - t_1$ is time interval, ξ indicates interpolation scheme: $\xi = 0$, forward interpolation (fully explicit); $\xi = 0.5$, linear interpolation (Crank–Nicolson), and $\xi = 1$, backwards interpolation (fully implicit). $\Delta x = x_2 - x_1 = x(t_2) - x(t_1)$.

Integration of Equation (22) using integration schemes (23) and (24) results in

$$\begin{bmatrix} G_{11} & G_{12} & G_{13} & G_{14} \\ G_{21} & G_{22} + \xi \Delta t K_{22} & G_{23} + \xi \Delta t K_{23} & G_{24} + \xi \Delta t K_{24} \\ G_{31} & G_{32} + \xi \Delta t K_{32} & G_{33} + \xi \Delta t K_{33} & G_{34} \\ G_{41} & G_{42} + \xi \Delta t K_{42} & G_{43} + \xi \Delta t K_{43} & G_{44} + \xi \Delta t K_{44} \end{bmatrix} \begin{Bmatrix} \Delta u \\ \Delta p_c \\ \Delta p_a \\ \Delta T \end{Bmatrix} = -\Delta t \begin{bmatrix} 0 & 0 & 0 & 0 \\ 0 & K_{22} & K_{23} & K_{24} \\ 0 & K_{32} & K_{33} & 0 \\ 0 & K_{42} & K_{43} & K_{44} \end{bmatrix} \begin{Bmatrix} u^{t_1} \\ p_c^{t_1} \\ p_a^{t_1} \\ T^{t_1} \end{Bmatrix} + \Delta t \begin{Bmatrix} 0 \\ F_2^{t_1} \\ F_3^{t_1} \\ F_4^{t_1} \end{Bmatrix} + \begin{Bmatrix} \Delta F_1 \\ \xi \Delta t \Delta F_2 \\ \xi \Delta t \Delta F_3 \\ \xi \Delta t \Delta F_4 \end{Bmatrix} \quad (25)$$

In the current study, ξ is chosen as 1 and lumped mass matrix is used to obtain stable solutions. u^{t_1} , $p_c^{t_1}$, $p_a^{t_1}$, T^{t_1} , $F_2^{t_1}$, $F_3^{t_1}$ and $F_4^{t_1}$ are values of u , p_c , p_a , T , F_2 , F_3 and F_4 at time t_1 . At every time step, an iterative procedure is used to update coefficient matrices in Equation (25) and solve for the increments of basic variables until the relative errors are within the specified limit.

From Equation (2), the time derivative of water content (θ) consists of three terms:

$$\frac{\partial \theta}{\partial t} = B_3 \frac{\partial \sigma^*}{\partial t} + B_4 \frac{\partial p_c}{\partial t} + B_5 \frac{\partial T}{\partial t} \quad (26)$$

where

$$B_3 = \frac{\partial \theta}{\partial \sigma^*}, \quad B_4 = \frac{\partial \theta}{\partial p_c}, \quad B_5 = \frac{\partial \theta}{\partial T}$$

Since mass balance errors in numerical solutions of pressure-based flow equations for isothermal rigid medium are attributed to the expansion of the time derivative of water content (or saturation) [24,25,27,28], it can be expected that the evaluation of B_3 , B_4 , and B_5 with analytical derivatives of water content cannot satisfy mass balance when the water retention curve of a non-isothermal deformable medium [Equation (2)] is non-linear. In other words, the tangent approximation of B_3 , B_4 and B_5 can be considered non-conservative. Mass-conservation is a necessary condition for numerical accuracy. In the following, two mass-conservative numerical techniques are developed to achieve better results. One is mass-conservation within each element, another is mass-conservation at each node.

3.1. Numerical scheme for mass-conservation within each element

Using the following interpolations to discretize Equation (26) for each element:

$$D_t \theta = \frac{d\theta}{dt} = \sum_{j=1}^{NN} N_j D_t \theta_j \tag{27}$$

$$B_3 D_t \sigma^* = B_3 \frac{d\sigma^*}{dt} = \sum_{j=1}^{NN} B_{3j} N_j D_t \sigma_j^* \tag{28}$$

$$B_4 D_t p_c = B_4 \frac{dp_c}{dt} = \sum_{j=1}^{NN} B_{4j} N_j D_t p_{cj} \tag{29}$$

$$B_5 D_t T = B_5 \frac{dT}{dt} = \sum_{j=1}^{NN} B_{5j} N_j D_t T_j \tag{30}$$

The finite element form of Equation (26) becomes

$$\int_{\Omega} N_i N_j d\Omega \begin{Bmatrix} D_t \theta_1 \\ \vdots \\ D_t \theta_{NN} \end{Bmatrix} = \int_{\Omega} B_{3j} N_i N_j d\Omega \begin{Bmatrix} D_t \sigma_1^* \\ \vdots \\ D_t \sigma_{NN}^* \end{Bmatrix} + \int_{\Omega} B_{4j} N_i N_j d\Omega \begin{Bmatrix} D_t p_{c1} \\ \vdots \\ D_t p_{cNN} \end{Bmatrix} + \int_{\Omega} B_{5j} N_i N_j d\Omega \begin{Bmatrix} D_t T_1 \\ \vdots \\ D_t T_{NN} \end{Bmatrix} \tag{31}$$

where NN is number of nodes in an element, Ω is the element domain, $D_t(\cdot) = d(\cdot)/dt$, N_i ($i = 1, \dots, NN$) is interpolating function. B_{3j} , B_{4j} and B_{5j} are values of B_3 , B_4 and B_5 at node j .

In order to preserve liquid water mass balance, the values of parameters B_{3j} , B_{4j} and B_{5j} have to satisfy Equation (31). One approach that satisfies this requirement is introducing a correction factor f_c as follows:

$$\int_{\Omega} N_i N_j \, d\Omega \begin{Bmatrix} D_t \theta_1 \\ \vdots \\ D_t \theta_{NN} \end{Bmatrix} = \int_{\Omega} f_{cj} \tilde{B}_{3j} N_i N_j \, d\Omega \begin{Bmatrix} D_t \sigma_1^* \\ \vdots \\ D_t \sigma_{NN}^* \end{Bmatrix} + \int_{\Omega} f_{cj} \tilde{B}_{4j} N_i N_j \, d\Omega \begin{Bmatrix} D_t p_{c1} \\ \vdots \\ D_t p_{cNN} \end{Bmatrix} + \int_{\Omega} f_{cj} \tilde{B}_{5j} N_i N_j \, d\Omega \begin{Bmatrix} D_t T_1 \\ \vdots \\ D_t T_{NN} \end{Bmatrix} \quad (32)$$

where

$$\tilde{B}_{3j} = \frac{B_{3j}}{f_{cj}} = \frac{\theta_j(\sigma^{*t2}, p_c^{t1}, T^{t1}) - \theta_j(\sigma^{*t1}, p_c^{t1}, T^{t1})}{\sigma^{*t2} - \sigma^{*t1}} \quad (33)$$

$$\tilde{B}_{4j} = \frac{B_{4j}}{f_{cj}} = \frac{\theta_j(\sigma^{*t1}, p_c^{t2}, T^{t1}) - \theta_j(\sigma^{*t1}, p_c^{t1}, T^{t1})}{p_c^{t2} - p_c^{t1}} \quad (34)$$

$$\tilde{B}_{5j} = \frac{B_{5j}}{f_{cj}} = \frac{\theta_j(\sigma^{*t1}, p_c^{t1}, T^{t2}) - \theta_j(\sigma^{*t1}, p_c^{t1}, T^{t1})}{T^{t2} - T^{t1}} \quad (35)$$

and σ^{*ij} , p_c^{ij} and T^{ij} ($j = 1, 2$) are values of σ^* , p_c and T at time instance t_j .

At every time interval in the finite element analysis, the left-hand side of Equation (32) is taken as known, and on the right-hand side only the values of f_{cj} ($j = 1, \dots, NN$) are unknown. Therefore f_{cj} can be solved from the NN equations (32). Finally, B_{3j} , B_{4j} and B_{5j} can be obtained from Equations (33)–(35). The use of these parameters in the finite element equations (25) serves to preserve the liquid water mass balance within each element. This is a necessary condition for obtaining accurate results, since failure to preserve mass balance could result in the accumulation of significant errors [25,28].

If one were to neglect the effect of deformation and temperature on the water retention curve, this approach could be reduced to the non-traditional mass balanced finite element chord slope scheme (fecsc) proposed by Abriola and Rathfelder [25] as a special case.

3.2. Numerical scheme for mass-conservation at each node

From Equation (26), water content variation at node j can be approximated as

$$\Delta \theta_j = B_{3j} \Delta \sigma_j^* + B_{4j} \Delta p_{cj} + B_{5j} \Delta T_j \quad (36)$$

Substitution of Equations (33)–(35) into (36) gives

$$\begin{aligned} \theta_j(\sigma^{*t2}, p_c^{t2}, T^{t2}) - \theta_j(\sigma^{*t1}, p_c^{t1}, T^{t1}) &= f_{cj} [\theta_j(\sigma^{*t2}, p_c^{t1}, T^{t1}) + \theta_j(\sigma^{*t1}, p_c^{t2}, T^{t1}) \\ &\quad + \theta_j(\sigma^{*t1}, p_c^{t1}, T^{t2}) - 3\theta_j(\sigma^{*t1}, p_c^{t1}, T^{t1})] \end{aligned} \quad (37)$$

therefore, f_{cj} can be calculated as

$$f_{cj} = \frac{\theta_j(\sigma^{*t2}, p_c^{t2}, T^{t2}) - \theta_j(\sigma^{*t1}, p_c^{t1}, T^{t1})}{[\theta_j(\sigma^{*t2}, p_c^{t1}, T^{t1}) + \theta_j(\sigma^{*t1}, p_c^{t2}, T^{t1}) + \theta_j(\sigma^{*t1}, p_c^{t1}, T^{t2}) - 3\theta_j(\sigma^{*t1}, p_c^{t1}, T^{t1})]} \quad (38)$$

Finally using Equations (33)–(35) to calculate B_{3j} , B_{4j} and B_{5j} . It is noted that the approximations of B_{3j} , B_{4j} and B_{5j} are continuous between elements and can be easily updated on a node-by-node basis.

In Equations (33)–(35), it is assumed that B_{3j} , B_{4j} and B_{5j} have the same correction factor f_{cj} . However, when one considers the different levels of water content non-linearity with respect to stress, capillary pressure and temperature, it could also be appropriate to assign a different weight to the correction factors for B_3 , B_4 and B_5 .

In addition to liquid water mass balance, the mass balance of soil medium also needs to be maintained. This can be achieved by adopting a similar procedure to that described above to evaluate the coefficients K , B_1 and B_2 .

4. NUMERICAL RESULTS

A finite element program was developed to implement the theory described above. This section presents solutions to three types of problems to demonstrate the salient features of the program: (1) isothermal infiltration, (2) heat conduction, and (3) non-isothermal water and heat transport in a rigid media. Comparisons are made with results from the literature to validate the program and verify the accuracy of the numerical technique. The fully coupled features of the theoretical model and the effects of temperature increase on desiccation and possible cracking due to tensile stresses in CCLs and GCLs will be further explored in a separate paper [29].

4.1. Isothermal infiltration into a dry soil

This problem involves vertical moisture infiltration into a 0.6 m dry soil column under constant surface ponding. The water retention curve for the soil is given by

$$\theta = \theta_r + \frac{\theta_s - \theta_r}{(1 + |\alpha\psi|^n)^m}, \quad \theta_r \leq \theta \leq \theta_s \quad (39)$$

where the residual water content $\theta_r = 0.102$, the saturated water content $\theta_s = 0.368$, $n = 2$ and $m = 0.5$. The hydraulic conductivity of the soil is given by

$$K_l = K_{sat} \frac{\{1 - (|\alpha\psi|^n)^{n-1} [1 + (|\alpha\psi|^n)]^{-m}\}^2}{(1 + |\alpha\psi|^n)^{m/2}} \quad (40)$$

where the saturated hydraulic conductivity of the soil $K_{sat} = 9.2 \times 10^{-5}$ m/s, $\alpha = 0.0335$ and $\psi = p_c/(\rho_1 g)$ is the capillary potential head.

The initial and boundary conditions are defined by

$$\begin{aligned} \psi(z, t = 0) &= -10m \\ \psi(z = 0, t) &= \psi_{bottom} = -10m \\ \psi(z = 0.6m, t) &= -0.75m \end{aligned} \quad (41)$$

The finite element solutions were obtained using 400 one-dimensional two-node elements of equal sizes. The initial time step was selected to be 0.1 s. This was increased when the number of iterations required for convergence dropped to less than 4. The maximum time step was 720 s.

Figure 2 shows the capillary potential distribution with the depth after 6 h. The three curves shown are: (1) the traditional finite element solution (tangent solution, not mass conservative), (2) the mass conservative finite element solution (present solution), and (3) semi-analytical solution (true solution) developed by Philip [30]. It can be seen that mass conservative finite element solution significantly improves the accuracy and agrees very well with the true solution.

4.2. Heat conduction in a slab

This example is to test the applicability of the model for heat conduction. The problem involves 5 m long slab with an initial uniform temperature of 20°C, thermal conductivity $\lambda = 2.89$ W/(m³K), and volumetric heat capacity $C = 3.2 \times 10^6$ J/(m³K). All other heat transport coefficients were set to zero. The boundary conditions are 50°C at one end and 20°C (unchanged) at the other end. The finite element solution was obtained using 100 uniform elements.

Figure 3 compares variation in temperature with time calculated from the finite element solution with the analytical solution [31] at three different locations (0.1 m, 1.0 m, 3.0 m). There is excellent agreement with the analytical solutions at all the locations over the entire time period.

4.3. Non-isothermal water and heat transport in a rigid media

The water retention curve and hydraulic conductivity for a clay liner at a reference temperature (T_0) can be described by van Genuchten–Mualem functions [14,32,33] as

$$\theta = \theta_r + \frac{\theta_s - \theta_r}{(1 + |\alpha\psi|^n)^m}, \quad \theta_r \leq \theta \leq \theta_s \quad (42)$$

$$\kappa_l = \kappa_{\text{sat}} \frac{[(1 + |\alpha\psi|^n)^m - |\alpha\psi|^{n-1}]^2}{(1 + |\alpha\psi|^n)^{m(l+2)}} \quad (43)$$

where θ_r is residual water content, θ_s is saturated water content, l , m and n are fitted parameters, and $m = 1 - 1/n$, $\psi (= p_c/\rho_l g)$ is capillary potential head at the reference temperature. κ_{sat} is the saturated mobility of liquid water in the porous media.

It has been suggested that temperature influences the water retention curve due to changes in surface tension, as well as changes in friction angle and soil texture [34]. However, in this example, due to limited experimental data, the effect of temperature on the water retention curve is considered through matric potential head correction. Therefore, for the non-isothermal unsaturated soil, the water retention curve can still be described by Equation (42), except that the variable ψ replaced by Ψ which represents a temperature corrected potential head which is assumed to be a function of capillary potential head and temperature [35]:

$$\Psi = \psi \exp[-C_\psi T] \quad (44)$$

where C_ψ is the temperature coefficient of water retention (°C⁻¹).

If the temperature dependence of water retention is only due to the change in surface tension then: $C_\psi = -0.002$ °C⁻¹ [12,14,15]. However, it is reported that, the surface tension model

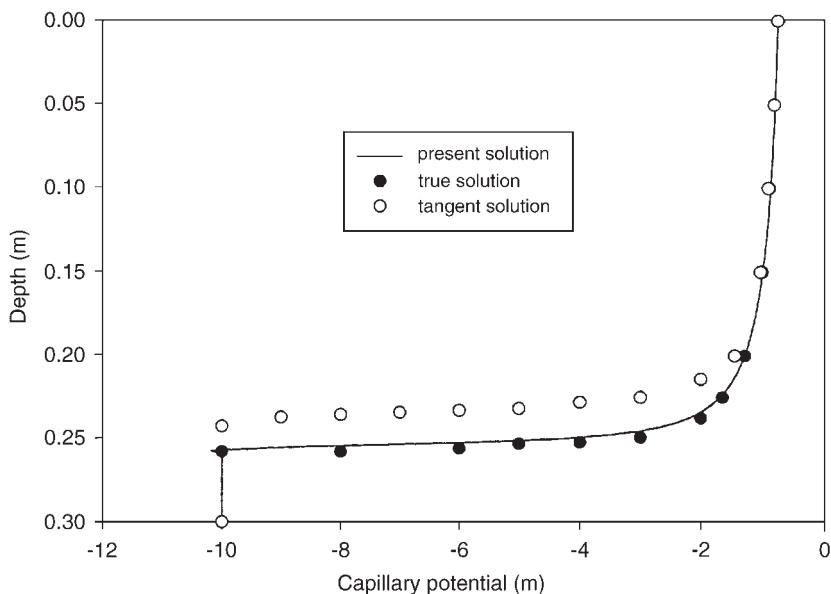


Figure 2. Capillary potential distribution after 6 h.

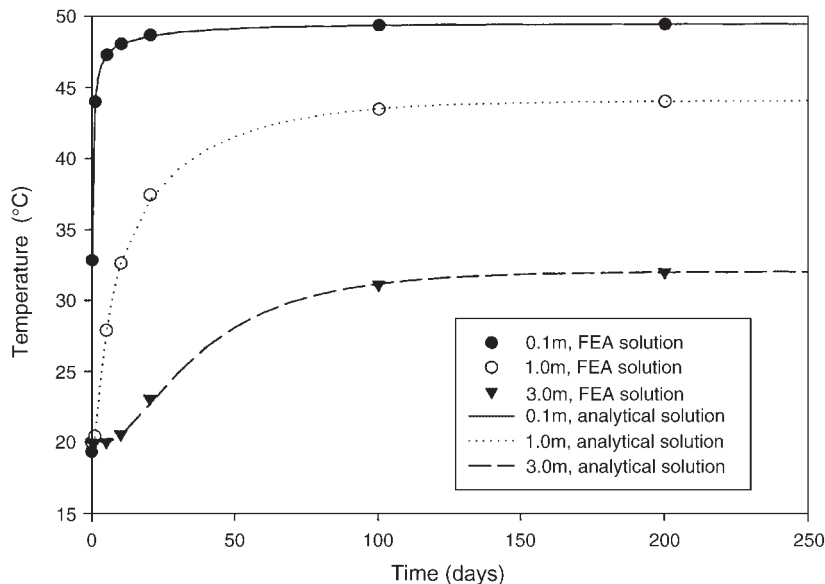


Figure 3. Comparison of finite element solutions with analytical solutions for heat conduction.

generally underestimates observed values of C_ψ by up to a factor of 8 [14,15,36]. Considering this factor, Scanlon and Milly [37] used $C_\psi = -0.0068 \text{ }^\circ\text{C}^{-1}$ in their study which produced reasonable results.

Table I. Material properties of the soil medium [14].

Soil	θ_r	θ_s	$\alpha(1/m)$	N	L	K_{sat} (m/s)	f_Q	f_{AM}	θ_k
Mineral liner	0.05	0.315	0.00058	1.05	0.5	1.4×10^{-9}	0.2	0.8	0.1
Sandstone layer	0	0.33	0.00054	1.32	0.5	8.1×10^{-8}	0.5	0.5	0.1

f_Q : volume of quartz per volume of soil solids. f_{AM} : volume of other minerals per volume of soil solids.

The mobility coefficient of water due to temperature change is given by [14]

$$\kappa_1 = \kappa_{\text{sat}} \frac{[(1 + |\alpha\Psi|^n)^m - |\alpha\Psi|^{n-1}]^2}{(1 + |\alpha\Psi|^n)^{m(l+2)}} e^{\kappa T} \quad (45)$$

where κ is the temperature coefficient of hydraulic conductivity. It should be noted that this approach may underestimate the sensitivity of hydraulic conductivity to temperature by a factor of 2 or 3 [38].

4.3.1. Non-isothermal drying of a mineral liner without infiltration. This example is to simulate the drying of the mineral base liners of a waste disposal site under the influence of a temperature gradient and has been selected because it has been previously examined by Schmidt and Bohne [39] and Döll [15]. Following the earlier work, the barrier system was assumed to consist of two layers: 0.6 m of compacted soil liner on top of a 0.5 m sandstone layer. The groundwater table is located at the bottom of the sandstone layer. The initial conditions are uniform matric potential head of -0.2 m and uniform temperature of 10°C in the soil medium. The temperature is then suddenly increased to 35°C at the upper boundary and to 28°C at the lower boundary. The top of the liner is impermeable (e.g. simulating the presence of a geomembrane). The material properties of the soil medium are given in Table I, and thermal properties can be calculated according to Appendix A.

This problem was solved using 55 uniform elements. The initial time step was set as 0.001 day. Figure 4 shows capillary potential head variation with depth after 7 years. Figure 5 shows volumetric water content variation with depth after 7 years. The solutions obtained by Schmidt and Bohne [39] and Döll [15] are also shown in Figures 4 and 5 for comparison. The present finite element solution is close to the other two solutions, except on the very top area where the present solution shows less loss of water. This difference could be a consequence of the different numerical methods adopted. Schmidt and Bohne [39] used a mixed finite element method, and Döll [15] used the finite difference method.

5. CONCLUSION

The objective of this paper was to develop a model capable of simulating the coupled heat-moisture-air transport in deformable unsaturated landfill liner system while adopting non-linear constitutive relationships. The governing equations for force equilibrium, water and air mass balance, and heat energy balance were derived in terms of displacement, capillary pressure, air pressure and temperature, and solved using the finite element method. Mass conservative numerical schemes were developed to improve the accuracy of numerical modelling. The model

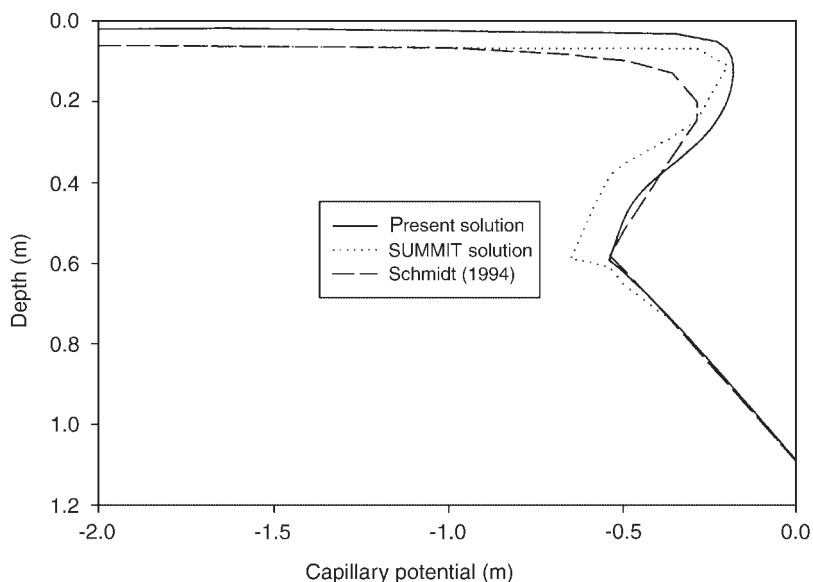


Figure 4. Capillary potential profile in a liner due to non-isothermal drying after 7 years.

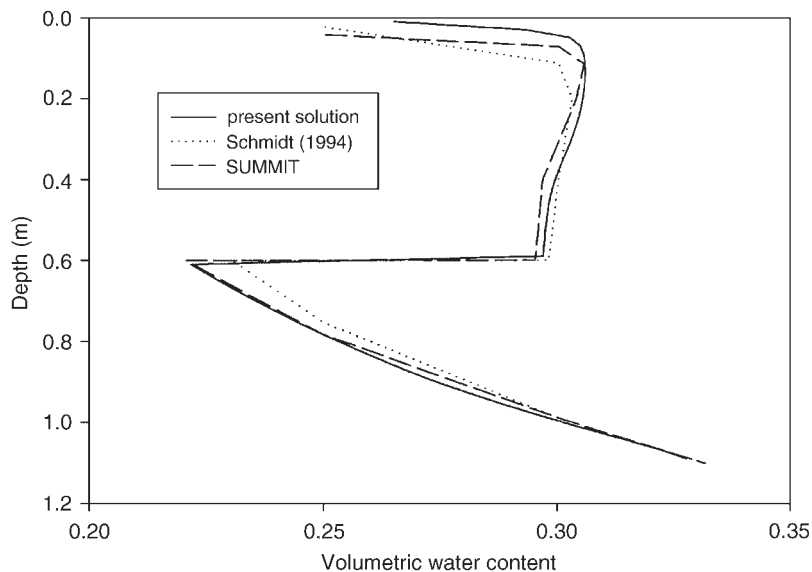


Figure 5. Water content distribution with depth after 7 years.

was tested against three types of problem and shown to provide good results. These test results have demonstrated that the current model is a general and fully coupled model, suitable for many different analyses, such as isothermal or non-isothermal, saturated or unsaturated, deformable or undeformable media.

A subsequent paper will describe the application of this model to study the fully coupled fields in two types of composite landfill liner. The stress and deformation are simultaneously calculated to facilitate the study of desiccation cracking, and a series of sensitivity analyses are presented for various parameters, such as hydraulic conductivity and thickness of the liner, to evaluate their effects on the service performance of the liner.

APPENDIX A: VARIABLES USED IN THE EQUATIONS

$$\begin{aligned}
 L_{11} &= \rho_1(\theta + B'_3), & L_{12} &= \rho_1 B'_4 + \rho_{10} \beta_1 \theta, & L_{13} &= \rho_{10} \beta_1 \theta, & L_{14} &= \rho_1 B'_5 - \rho_{10} \alpha_1 \theta \\
 L_{21} &= \rho_v(1 - \theta - B'_3), & L_{22} &= -\rho_v B'_4 + (n - \theta) \frac{D_1^*}{D^*} \\
 L_{23} &= (n - \theta) \frac{D_2^*}{D^*}, & L_{24} &= -\rho_v B'_5 + (n - \theta) \frac{D_3^*}{D^*} \\
 L_{31} &= \rho_{da}[1 - (1 - H)(\theta + B'_3)], & L_{32} &= -\{(1 - H)\rho_{da} B'_4 + [n - (1 - H)\theta] \frac{R_v D_1^*}{R_{da} D^*}\} \\
 L_{33} &= [n - (1 - H)\theta] \left[\frac{1}{R_{da} T_K} - \frac{R_v D_2^*}{R_{da} D^*} \right] \\
 L_{34} &= -\left\{ (1 - H)\rho_{da} B'_5 + [n - (1 - H)\theta] \left[\frac{p_a}{R_{da} T_K^2} + \frac{R_v D_3^*}{R_{da} D^*} \right] \right\} \\
 L_{41} &= \left[\theta + B'_3 \left(1 - \frac{\theta}{\delta S} \right) \right] \frac{H_w}{\delta} e^{-\theta/\delta S} - (T + T_0)KB_2 + C_1 TL_{11} + (L_0 + C_v T)L_{21} + C_{da} TL_{31} \\
 L_{42} &= B'_4 \left(1 - \frac{\theta}{\delta S} \right) \frac{H_w}{\delta} e^{-\theta/\delta S} + C_1 TL_{12} + (L_0 + C_v T)L_{22} + C_{da} TL_{32} \\
 L_{43} &= C_1 TL_{13} + (L_0 + C_v T)L_{23} + C_{da} TL_{33} \\
 L_{44} &= (\rho C)_m^* + B'_5 \left(1 - \frac{\theta}{\delta S} \right) \frac{H_w}{\delta} e^{-\theta/\delta S} + C_1 TL_{14} + (L_0 + C_v T)L_{24} + C_{da} TL_{34}
 \end{aligned}$$

H_w , δ and S are material properties related to differential heat of wetting W [35].

$$B'_3 = B_3 K, \quad B'_4 = B_4 - B_1 B_3 K, \quad B'_5 = B_5 - B_2 B_3 K$$

$$D_{c2}^* = (\rho_1 \kappa_1 C_1 + D_1^* C_v + C_{da} \kappa_1 \rho_{da} H) T + L_0 D_1^*$$

$$D_{a2}^* = [\rho_1 \kappa_1 C_1 + (\rho_v \kappa_a + D_2^*) C_v + C_{da} \rho_{da} (\kappa_a + \kappa_1 H)] T + L_0 (\rho_v \kappa_a + D_2^*)$$

$$D_{T2}^* = D_3^* (L_0 + C_v T) + \lambda' = D_3^* C_1 T + \lambda$$

Density of saturated water vapour ρ_0 is given by [40]

$$\rho_0 = 0.001 \exp(19.819 - 4975.9/T_K) \quad (\text{kg/m}^3)$$

Diffusion coefficient D^* in the porous medium can be expressed as

$$D^* = f(\theta)\tau D_{atm}(T, p_a)$$

where $f(\theta)$ is effective porosity for vapour diffusion given by [12]

$$f(\theta) = \begin{cases} n_p & \theta \leq \theta_k \\ (n_p - \theta) \left(1 + \frac{\theta}{n_p - \theta_k} \right) & \theta > \theta_k \end{cases}$$

n_p is porosity.

τ is tortuosity given by [41]

$$\tau = (n_p - \theta)^{0.66}$$

D_{atm} is vapour diffusion coefficient in free air given by [42]

$$D_{atm} = 2.17 \times 10^{-5} \frac{101326}{p_a} \left(\frac{T_K}{273.15} \right)^{1.88} \quad (m^2/s)$$

$$D_1^* = f(\theta)\tau D_{atm} \rho_v \left[\frac{1}{\rho_l R_v T_K} - \frac{p_c \rho_{l0} \beta_l}{\rho_l^2 R_v T_K} \right]$$

$$D_2^* = - f(\theta)\tau D_{atm} \frac{\rho_v p_c \rho_{l0} \beta_l}{\rho_l^2 R_v T_K}$$

$$D_3^* = F_v \xi(\theta) f(\theta) D_{atm} \left[h \frac{d\rho_0}{dT} - \frac{\rho_v p_c}{\rho_l R_v T_K^2} + \frac{\rho_v p_c \rho_{l0} \alpha_l}{\rho_l^2 R_v T_K} \right]$$

$\xi(\theta)$ is the temperature gradient ratio accounting for the fact that temperature gradient in gas(air)-filled pores is larger than the bulk temperature gradient, which enhances vapour transport.

According to de Vries [43] and Milly [35]:

$$\xi(\theta) = \begin{cases} \frac{k_2}{\sum_{i=1}^5 k_i \theta_i} & \theta \geq \theta_k \\ 1 + \frac{\xi(\theta_k) - 1}{\theta_k} \theta & \theta < \theta_k \end{cases}$$

and

$$k_i = \begin{cases} \frac{2}{3} \frac{1}{(\lambda_i/\lambda - 1)g_i} + \frac{1}{3} \frac{1}{1 + (\lambda_i/\lambda - 1)(1 - 2g_i)} & i = 2, 3, 4, 5 \\ 1 & i = 1 \end{cases}$$

θ_k is minimum water content where liquid continuity exists, g_i is shape factor of the corresponding soil constituents (see Table AI).

$$\lambda_v = D_{atm} L(T) \left. \frac{\partial \rho_v}{\partial T} \right|_{p_c}$$

Table AI. Volumetric heat capacities, thermal conductivities and shape factors of the five soil constituents [15].

Constituent	i	$c_i[\text{J}/(\text{m}^3\text{K})]$	$C_i[\text{J}/(\text{m}^3\text{K})]$	$\lambda_i[\text{W}/(\text{mK})]$	g_i
Liquid water	1	4.19×10^3		0.57	
Air + vapour	2	1.86×10^3		$\lambda_a + \lambda_v = 0.025 + \lambda_v$	$0.035 + 0.298\theta/n_p$
quartz	3		2.0×10^6	8.8	0.125
Other minerals	4		2.0×10^6	2.0	0.125
Organic matter	5		2.5×10^6	0.25	0.5

$$L(0^\circ\text{C}) = 2.5016 \times 10^6 \text{ J/kg}$$

$$L(T) = L(0^\circ\text{C}) - (c_1 - c_v)T = 2.5016 \times 10^6 - 2330T \text{ J/kg}$$

Effective thermal conductivity λ can be calculated by [43]:

$$\lambda(\theta) = \begin{cases} \frac{\sum_{i=1}^5 k_i \theta_i \lambda_i}{\sum_{i=1}^5 k_i \theta_i} & \theta \geq \theta_k \\ \lambda(0) + \frac{\lambda(\theta_k) - \lambda(0)}{\theta_k} \theta & \theta < \theta_k \end{cases}$$

$$\lambda(0) = 1.25 \frac{n_p \lambda_a + \sum_3^5 k_i \theta_i \lambda_i}{n_p + \sum_3^5 k_i \theta_i}$$

and k_i determined as above, but with λ_2 , not λ_1 .

APPENDIX B: COMPONENTS OF MATRICES G, K, F

$$\begin{aligned} G_{11} &= \int_{\Omega} \mathbf{B}^T \mathbf{D} \mathbf{B} \, d\Omega, & G_{12} &= - \int_{\Omega} \mathbf{B}^T \mathbf{K} B_1 \mathbf{m}^T \mathbf{N} \, d\Omega, \\ G_{13} &= - \int_{\Omega} \mathbf{B}^T \mathbf{m}^T \mathbf{N} \, d\Omega, & G_{14} &= - \int_{\Omega} \mathbf{B}^T \mathbf{K} B_2 \mathbf{m}^T \mathbf{N} \, d\Omega \\ G_{21} &= \int_{\Omega} \mathbf{N}^T (L_{11} + L_{21}) \mathbf{m} \mathbf{B} \, d\Omega, & G_{22} &= \int_{\Omega} \mathbf{N}^T (L_{12} + L_{22}) \mathbf{N} \, d\Omega \\ G_{23} &= \int_{\Omega} \mathbf{N}^T (L_{13} + L_{23}) \mathbf{N} \, d\Omega, & G_{24} &= \int_{\Omega} \mathbf{N}^T (L_{14} + L_{24}) \mathbf{N} \, d\Omega \\ G_{31} &= \int_{\Omega} \mathbf{N}^T L_{31} \mathbf{m} \mathbf{B} \, d\Omega, & G_{32} &= \int_{\Omega} \mathbf{N}^T L_{32} \mathbf{N} \, d\Omega \\ G_{33} &= \int_{\Omega} \mathbf{N}^T L_{33} \mathbf{N} \, d\Omega, & G_{34} &= \int_{\Omega} \mathbf{N}^T L_{34} \mathbf{N} \, d\Omega \end{aligned}$$

$$\begin{aligned}
G_{41} &= \int_{\Omega} \mathbf{N}^T L_{41} \mathbf{m} \mathbf{B} \, d\Omega, & G_{42} &= \int_{\Omega} \mathbf{N}^T L_{42} \mathbf{N} \, d\Omega \\
G_{43} &= \int_{\Omega} \mathbf{N}^T L_{43} \mathbf{N} \, d\Omega, & G_{44} &= \int_{\Omega} \mathbf{N}^T L_{44} \mathbf{N} \, d\Omega \\
K_{22} &= \int_{\Omega} \nabla \mathbf{N}^T (\rho_1 \kappa_1 + D_1^*) \nabla \mathbf{N} \, d\Omega, & K_{23} &= \int_{\Omega} \nabla \mathbf{N}^T (\rho_1 \kappa_1 + \rho_v \kappa_a + D_2^*) \nabla \mathbf{N} \, d\Omega \\
K_{24} &= \int_{\Omega} \nabla \mathbf{N}^T D_3^* \nabla \mathbf{N} \, d\Omega, & K_{32} &= \int_{\Omega} \nabla \mathbf{N}^T H \rho_{da} \kappa_1 \nabla \mathbf{N} \, d\Omega \\
K_{33} &= \int_{\Omega} \nabla \mathbf{N}^T \rho_{da} (\kappa_a + H \kappa_1) \nabla \mathbf{N} \, d\Omega, & K_{42} &= \int_{\Omega} \nabla \mathbf{N}^T D_{c2}^* \nabla \mathbf{N} \, d\Omega \\
K_{43} &= \int_{\Omega} \nabla \mathbf{N}^T D_{a2}^* \nabla \mathbf{N} \, d\Omega, & K_{44} &= \int_{\Omega} \nabla \mathbf{N}^T D_{T2}^* \nabla \mathbf{N} \, d\Omega \\
F_1 &= \int_{\Gamma} \mathbf{N}^T \mathbf{t} \, d\Gamma, & F_2 &= \int_{\Gamma} \mathbf{N}^T (\mathbf{q}_1 + \mathbf{q}_v) \, d\Gamma - \int_{\Omega} \nabla \mathbf{N}^T \rho_1 \kappa_1 \nabla (\rho_1 g z) \, d\Omega \\
F_3 &= \int_{\Gamma} \mathbf{N}^T \mathbf{q}_{da} \, d\Gamma - \int_{\Omega} \nabla \mathbf{N}^T H \rho_{da} \kappa_1 \nabla (\rho_1 g z) \, d\Omega \\
F_4 &= \int_{\Gamma} \mathbf{N}^T \mathbf{q}_T \, d\Gamma - \int_{\Omega} \nabla \mathbf{N}^T (C_1 \rho_1 + C_{da} \rho_{da} H) \kappa_1 T \nabla (\rho_1 g z) \, d\Omega
\end{aligned}$$

where $\mathbf{m} = \langle 1 \ 1 \ 0 \rangle$ for 2-D condition, and $\langle 1 \rangle$ for 1-D condition.

ACKNOWLEDGEMENTS

The financial support of the Natural Sciences and Engineering Research Council of Canada (NSERC), Terrafix Geosynthetic Inc., and the Centre for Research in Earth and Space Technology (CRESTech) is gratefully acknowledged.

REFERENCES

1. Rowe RK, Quigley RM, Booker JR. *Clayey Barrier Systems for Waste Disposal Facilities*. E.&F.N. Spon Ltd. (Chapman Hall): London, U.K. 1995.
2. Rowe RK. Geosynthetics and the minimization of contaminant migration through barrier systems beneath solid waste. Keynote lecture for the *6th International Conference on Geosynthetics*, Atlanta, GA, 1998; 27–102.
3. Rowe RK. Liner Systems, *Geotechnical and Geoenvironmental Engineering Handbook*, Chapter 25. Kluwer Academic Publishing: Norwell, U.S.A., 2001; 739–788.
4. Collins HJ. Impact of the temperature inside the landfill on the behaviour of barrier systems. *Proceedings of Fourth International Landfill Symposium*, Cagliari, Italy, 1993; 417–432.
5. Heibroek G, Jessberger HL. Safety analysis of a composite liner system. *Proceedings of Fourth International Landfill Symposium*, Cagliari, Italy, 1995; 169–183.
6. Yoshida H, Tanaka N, Hozumi H. Theoretical study on heat transport phenomena in a sanitary landfill. *Proceedings of Sixth International Landfill Symposium*, vol. 1. Cagliari, Italy, 1997; 110–119.
7. Barone FS, Costa JMA, Ciardullo L. Temperature at the base of a Municipal Solid Waste Landfill. *50th Canadian Geotechnical Conference*, Ottawa, October, vol. 1, 1997; 144–152.
8. Abu-Hejleh AN, Znidarcic D. Desiccation theory for soft cohesive soils. *Journal of Geotechnique and Engineering* 1995; **121**:493–502.
9. Lee FH, Lo KW, Lee SL. Tension crack development in soils. *Journal of Geotechnique and Engineering*, ACSE 1988; **114**:915–929.
10. Morris PH, Graham J, Williams DJ. Cracking in drying soils. *Canadian Geotechnical Journal* 1992; **29**:263–272.

11. Konrad J-M, Ayad R. An idealized framework for the analysis of cohesive soils undergoing desiccation. *Canadian Geotechnical Journal* 1997; **34**:477–488.
12. Philip JR, de Vries DA. Moisture movement in porous materials under temperature gradients. *Transactions of the American Geophysical Union* 1957; **38**:222–232.
13. Milly PCD. Moisture and heat transport in hysteric, inhomogeneous porous media: a heat-based formulation and a numerical model. *Water Resources Research* 1982; **18**:489–498.
14. Döll P. Desiccation of mineral liners below landfills with heat generation. *Journal of Geotechnical and Geoenvironmental Engineering* 1996; **123**:1001–1009.
15. Döll P. Modeling of moisture movement under the influence of temperature gradients: desiccation of mineral liners below landfills. *Ph.D. Thesis*, Technical University of Berlin, Germany, 1996.
16. Heibrock G. Decision cracking of mineral sealing liners. *Proceedings of Sixth International Landfill Symposium*, vol. 3, Cagliari, Italy, 1997; 101–113.
17. Dakshnamurthy V, Fredlund DG. A mathematical model for predicting moisture flow in an unsaturated soil under hydraulic and temperature gradient. *Water Resources Research* 1981; **17**:714–722.
18. Geraminegad M, Saxena SK. A coupled thermoelastic model for saturated-unsaturated porous media. *Geotechnique* 1986; **36**:539–550.
19. Navarro V, Gens A, Lloret A, Alonso EE. Development of a computer code for the analysis of coupled thermo-hydro-mechanical boundary value problems. *3rd International Workshop on Clay Barriers*, Bergamo, Italy, 1993.
20. Thomas HR, He Y. Analysis of coupled heat, moisture and air transfer in a deformable unsaturated soil. *Journal of Engineering Mechanics, ASCE* 1995; **121**:392–405.
21. Yang DQ, Rahardjo H, Leong EC, Choa V. Coupled model for heat, moisture, air flow, and deformation problems in unsaturated soils. *Journal of Engineering Mechanics, ASCE* 1998; **124**:1331–1338.
22. Zhou Y, Rajapakse RKND, Graham J. Coupled heat-moisture-air transfer in deformable unsaturated media. *Journal of Engineering Mechanics, ASCE*, 1998; **124**:1090–1099.
23. Thomas HR, He Y, Sansom MR, Li CLW. On the development of a model of the thermo-mechanical-hydraulic behaviour of unsaturated soils. *Engineering Geology* 1996; **41**:197–218.
24. Celia MA, Boulouton ET, Zarba RL. A general mass conservation numerical solution for the unsaturated flow equation. *Water Resources Research* 1990; **26**:1483–1496.
25. Abriola LM, Rathfelder K. Mass balance errors in modelling two-phase immiscible flows: Causes and remedies. *Advances in Water Resource* 1993; **16**:223–239.
26. Sisler HH, Vanderwerf CA, Davidson AW. *General Chemistry—A systematic Approach*. Macmillan: New York, 1953.
27. Aziz K, Settari A. *Petroleum Reservoir Simulation*. Applied Science Publishers: London, 1979.
28. Milly PCD. A mass conservative procedure for time-stepping in models of unsaturated flow. *Advances in Water Resources* 1985; **8**:32–36.
29. Zhou Y, Rowe RK. Modelling of clay liner desiccation. *Research Report R102*, GeoEngineering Centre, Queen's University, Kingston, ON, Canada.
30. Philip JR. (1969) Theory of infiltration. In *Advances in Hydroscience*, Chow VT (ed.), vol. 5. Academic: Sandiego, Calif. 1969; 215–305.
31. Carslaw HS, Jaeger JC. *Conduction of Heat in Solids* (2nd edn). Clarendon Press: Oxford, 1959.
32. van Genuchten MT. A closed-form equation for predicting the hydraulic conductivity of unsaturated soils. *Soil Science Society of America, Journal* 1980; **44**:892–898.
33. Mualem Y. A new model for predicting the hydraulic conductivity of unsaturated porous media. *Water Resources Research* 1976; **12**:1248–1254.
34. She HY, Sleep BE. The effect of temperature on capillary pressure-saturation relationships for air-water and perchloroethylene-water systems. *Water Resources Research* 1998; **34**:2587–2597.
35. Milly PCD. A simulation analysis of thermal effects on evaporation from soil. *Water Resources Research* 1984; **20**:1087–1098.
36. Nimmo JR, Miller EE. The temperature dependence of isothermal moisture versus potential characteristics of soils. *Soil Science Society of America, Journal* 1986; **50**:1105–1113.
37. Scanlon BR, Milly PCD. Water and heat fluxes in desert soils, 2. Numerical simulations. *Water Resources Research* 1994; **30**: pp. 721–733.
38. Giakoumakis SG, Tsakiris GP. Eliminating the effect of temperature from unsaturated soil hydraulic functions. *Journal of Hydrology* 1991; **129**:109–125.
39. Schmidt M, Bohne K. Simulation von Wasser- und Dampftransport in Deponiebasisabdichtungssystemen unter Berücksichtigung von Auflast und Temperaturgradienten. In *BMBF-Verbundforschungsvorhaben Weiterentwicklung von Deponieabdichtungssystemen*, 3. Arbeitstagung März 1993. August H, Holzlohner U, Meggyes T (eds). Bundesanstalt für Materialforschung und -prüfung Berlin 1995; 221–234.
40. Kimball BA, Jackson RD, Reginato RJ, Nakayama FS, Idso SB. Comparison of field measured and calculated soil heat fluxes. *Soil Science Society of America, Journal* 1976; **40**:18–25.

41. Lai S, Tiedje JM, Erickson AE. In situ measurement of gas diffusion coefficients in soils. *Soil Science Society of America, Journal* 1976; **40**:3–6.
42. De Vries DA, Kruger AJ. On the value of the diffusion coefficient of water vapor in air. In Phenomenes de transport avec changement de phase dans les milieux poreux ou colloïdaux, *Proceedings of CNRS Symposium*, vol. 160, Paris. Centre National de la Recherche Scientifique, Paris, 1967; 61–72.
43. De Vries DA. Thermal properties of soils. In *Physics of Plant Environment*, Wijk WR (ed.). John Wiley & Sons, Inc.: New York, 1963; 210–235.